Chapter 5

Loss modelling

Losses in an electric machine cause an increase in temperature. Whenever thermal modelling is done, loss modelling is equally important to obtain the location and values of the loss sources. In this chapter, the dominant loss mechanisms found in high speed, slotless PMSMs is discussed.

5.1 Introduction

Section 2.7 introduced the losses found in electric machines, especially high speed slotless PMSMs. Conduction loss is found in the stator winding and is caused by the externally applied voltage source connected to the winding. Eddy current losses are found in the stator winding, stator lamination, shielding cylinder, PM and rotor laminations. Hysteresis losses are found in the stator laminations and rotor laminations. Both eddy current and hysteresis losses are caused by a varying magnetic field. In the stator, the varying magnetic field is mainly due to the PM rotation, thus a 2-D magnetic model is required. An analytical 2-D magnetic model is derived in the next section. This is then used to determine the stator iron and winding losses.

The eddy current loss in the shielding cylinder and PM are caused by the varying magnetic field due to harmonic currents flowing in the stator winding. Section 5.5 discusses a simple resistive approach to calculating the eddy currents. It can also be done using analytical methods as demonstrated by Holm [13]. This chapter also discusses the mechanical losses, i.e., bearing and windage losses.

5.2 Magnetic field model

The eddy current and hysteresis losses in the stator laminations are caused by the changing magnetic field, due to the rotation of the rotor. The magnetic field distribution can be calculated using analytical or numerical methods. The TWINS machines are slotless PMSMs with a solid PM on the rotor and can be modelled magnetically in four layers as shown in Figure 5.1. The rotor laminations and shaft are combined in region 1, were $0 < r \leq r_{pmi}$. Only the magnetic field due to the PM will be modelled, thus the winding and coil former can be modelled as air, resulting in the large air gap region (layer 3), where $r_{agi} \leq r \leq r_{sli}$. The stator laminations are layer 4, where $r_{sli} \leq r \leq r_{slo}$, and the PM is layer 2, where $r_{pmi} \leq r \leq r_{agi}$. The permeability of the layers is also shown in Figure 5.1. The air gap and PM have a relative permeability of 1 and 1.05, respectively, which is much smaller than the relative permeability of the laminations. To simplify the model, it is assumed that the laminations have an infinite permeability. This assumption will be verified when comparing the analytical model's results with a FEM model. It is also assumed that the relative permeability of the PM is 1.

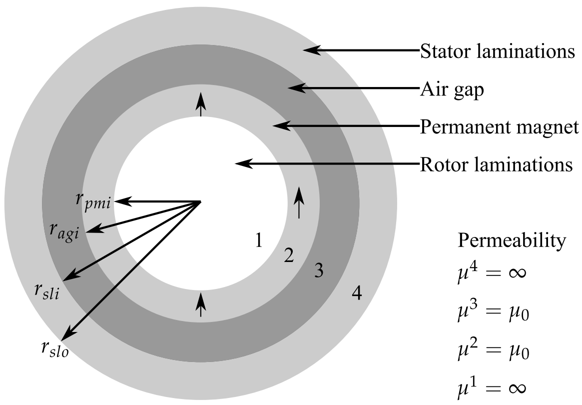

Figure 5.1: Machine simplification for magnetic field calculation

In all the layers, the governing equation is:

$$\nabla^2 \mathbf{A} = 0 \tag{5.1}$$

where $\mathbf{A}$ is the magnetic vector potential. For this senario, the general solution is

$$A_z^v(r, \phi) = \left[C_v r + D_v \frac{1}{r} \right] cos(\phi) \tag{5.2}$$

where v is the layer number and C_v,D_v are constants that will be determined from the boundary conditions. The first boundary condition is a result of Gauss's Law for conservation of magnetic flux $\mathbf{B}$:

$$\nabla . \mathbf{B} = 0 \tag{5.3}$$

and states that the normal component of the flux density in one region must equal that in a neighboring region, or:

$$\hat{\mathbf{n}} . (\mathbf{B}^v - \mathbf{B}^{v+1}) = 0. \tag{5.4}$$

where $\hat{\mathbf{n}}$ is the unit normal vector. The second boundary condition is a result of Ampere's Law:

$$\nabla \times \mathbf{H} = \mathbf{J} \tag{5.5}$$

where $\mathbf{H}$ is the magnetic field intensity and $\mathbf{J}$ is the current density. The boundary condition is:

$$\hat{\mathbf{n}} \times (\mathbf{H}^v - \mathbf{H}^{v+1}) = \mathbf{K}^v, \tag{5.6}$$

or the tangential component of the magnetic field intensity on one side is equal to that on the neighboring side plus the surface current density between them ($\mathbf{K}^v$). Applying (5.4) and (5.6) in all the layers, the constants are:

$$\begin{bmatrix} C_1 \\ C_2 \\ D_2 \\ C_3 \end{bmatrix} = \begin{bmatrix} -\dfrac{\hat{B}_{rem}(r_{pmi}^2 - r_{agi}^2)}{r_{pmi}^2 - r_{sli}^2} \\ -\dfrac{\hat{B}_{rem}(-r_{sli}^2 + 2r_{pmi}^2 - r_{agi}^2)}{2(-r_{sli}^2 + r_{pmi}^2)} \\ \dfrac{\hat{B}_{rem} r_{pmi}^2 (r_{agi}^2 - r_{sli}^2)}{2(-r_{sli}^2 + r_{pmi}^2)} \\ -\dfrac{\hat{B}_{rem}(r_{pmi}^2 - r_{agi}^2)}{2(-r_{sli}^2 + r_{pmi}^2)} \end{bmatrix}, \begin{bmatrix} D_3 \\ C_4 \\ D_4 \end{bmatrix} = \begin{bmatrix} -\dfrac{\hat{B}_{rem}(r_{pmi}^2 - r_{agi}^2) r_{sli}^2}{2(-r_{sli}^2 + r_{pmi}^2)} \\ \dfrac{\hat{B}_{rem}(r_{pmi}^2 - r_{agi}^2) r_{sli}^2}{(-r_{sli}^2 + r_{pmi}^2)(r_{slo}^2 - r_{sli}^2)} \\ -\dfrac{\hat{B}_{rem}(r_{pmi}^2 - r_{agi}^2) r_{sli}^2 r_{slo}^2}{(-r_{sli}^2 + r_{pmi}^2)(r_{slo}^2 - r_{sli}^2)} \end{bmatrix} \quad (5.7)$$

where $\hat{B}_{rem}$ is the maximum remanent flux density of the PM. Figure 5.2 shows a contour plot of the magnetic vector potential of the TWINS machine. The magnetic flux density in the r and ϕ directions are shown in Figure 5.3 at various radii: winding inside (r_{wi}), winding center (r_{wc}), stator inside (r_{si}) and stator center (r_{sc}). The maximum flux density will be used in the loss calculation in the stator and winding due to the PM magnetic field. The analytic field model is verified using COMSOL® Multiphysics® and the maximum difference is less than 2%. The difference can be attributed to the assumption that the stator permeability is assumed infinite in the analytic model.

5.3 Stator iron losses

Assuming the change in flux density in the stator laminations is influenced mostly by the PM, the hysteresis and eddy current losses in the stator laminations can be calculated using the

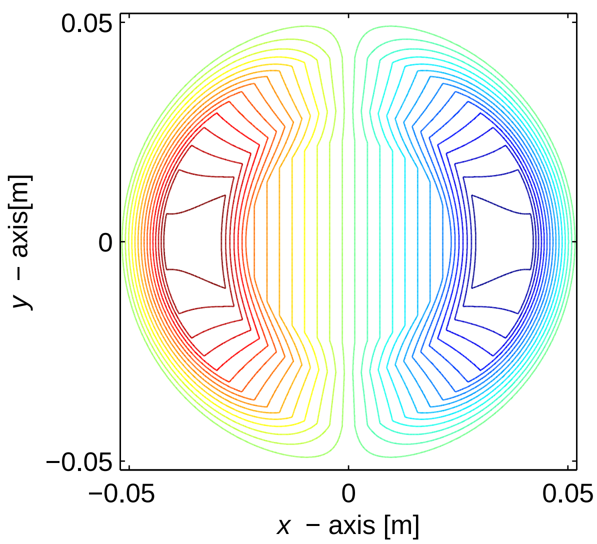

Figure 5.2: Contour plot of the magnetic vector potential of the TWINS

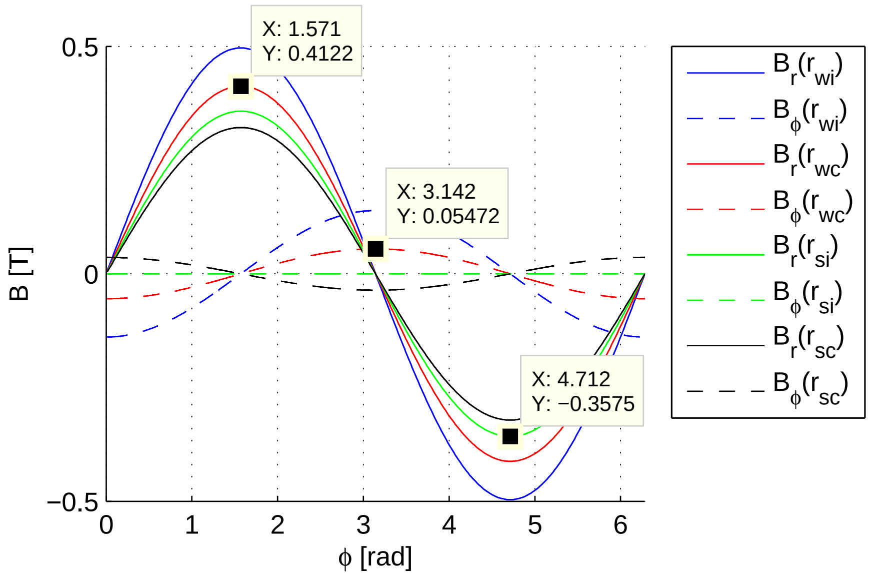

Figure 5.3: Magnetic flux density in the TWINS

results from the previous section and datasheet information.

The maximum magnetic flux density $\hat{B}$ inside the laminations is 0.3575 T, the maximum of $B_r(r_{si})$ as shown in Figure 5.3. Since the TWINS are two pole machines, the electric and mechanical frequency will be equal: 500 Hz at 30000 r/min. The mass of the stator laminations is calculated from the dimensions and density (7600 kg/m^2) as 1.21 kg if the stacking factor is assumed to be 0.9. Polinder proposed that the material data can be used to calculate the iron loss per mass unit (k_{Fe}) [131]:

$$k_{Fe} = c_{Fe,0} k_{Fe,0} \left(\frac{f}{f_0}\right)^{1.5} \left(\frac{\hat{B}}{\hat{B}_0}\right)^2 \tag{5.8}$$

where $k_{Fe,0}$ is the specific iron loss at a frequency f_0 and magnetic flux density $\hat{B}_0$ and $c_{Fe,0}$ is a dimensionless empirical correlation factor. From the datasheet for M270-35A, the total iron loss ($P_{s,Fe}$) can be calculated for 30000 r/min rotational speed, as shown in Table 5.1. This includes hysteresis and eddy current losses in the stator laminations. This result is based on the assumption that the flux density in the whole stator lamination equals the flux density at the inside surface. This assumption represents the worst case senario.

Table 5.1: Iron loss at 30000 r/min

f [Hz]	f_0 [Hz]	$\hat{B}$ [T]	$\hat{B}_0$ [T]	$k_{fe,0}$ [W/kg]	$c_{Fe,0}$	k_{Fe} [W/kg]	$P_{s,Fe}$ [W]
500	400	0.35	0.4	3.33	2	7.12	8.62

5.4 Stator winding eddy current loss

The stator winding loss can be calculated using analytical or numerical methods.

5.4.1 Analytical model

The changing magnetic field will induce eddy currents in the stator windings. The eddy current loss in the stator windings ($P_{s,Cu,e}$) can be calculated using [13]:

$$P_{s,Cu,e} = \frac{1}{8}\omega^2 r_{strand}^2 \sigma \left(\hat{B}_r^2 + \hat{B}_\phi^2 \right) A_{Cu} l_s \tag{5.9}$$

where r_{strand} is the radius of a strand, σ is the electrical conductivity of the strand, A_{Cu} is the total copper area of the winding, l_s is the strand length and $\hat{B}_r$ and $\hat{B}_\phi$ are the maximum values of the magnetic flux in the radial and tangential directions, respectively. In the TWINS, 30 strands of 0.2 mm radius wire were used per turn and 26 turns formed one of the three phases, resulting in 4680 conductors found in the cross-section of the machine. The total area is then $A_{Cu} = 0.588 \times 10^{-3}$ m^2 and the active length (l_s) is 0.06 m. From the magnetic field solutions, $\hat{B}_r = 0.4122$ T and $\hat{B}_\phi = 0.0547$ T in the center of the winding. The conductivity of copper is $\sigma = 58 \times 10^6$ S/m at 293.15 K. The eddy current loss induced in the winding is calculated as 17.45 W at 30000 r/min.

5.4.2 FEM model

The eddy current loss in the stator windings can also be determined using FEM. By modelling the moving PM, the current density in a conductor in the center of the winding is shown in Figure 5.4. The eddy current loss for one rotation is shown is Figure 5.5. As expected, the loss is a maximum when there is a maximum change in magnetic flux through the conductor. This occurs twice in one rotation since the rotor has a magnetic north and south pole. The average loss calculated using FEM at 30000 r/min is 18.8 W. There is a good correlation between the analytical and numerical results of the winding eddy current loss.

5.5 Shielding cylinder eddy current loss

5.5.1 Background

Eddy current loss has been researched for decades and has always been one of the important loss components whenever a changing magnetic field is involved. The goal of this section is not a thorough literature survey, but rather to show that rotor eddy current calculation remains a challenging and important part of PMSM design.

Atkinson *et al.* used 3-D and 2-D FEM to calculate the rotor eddy current loss [108]. Including end effects can only be done when using 3-D FEM, but this requires extremely long solution

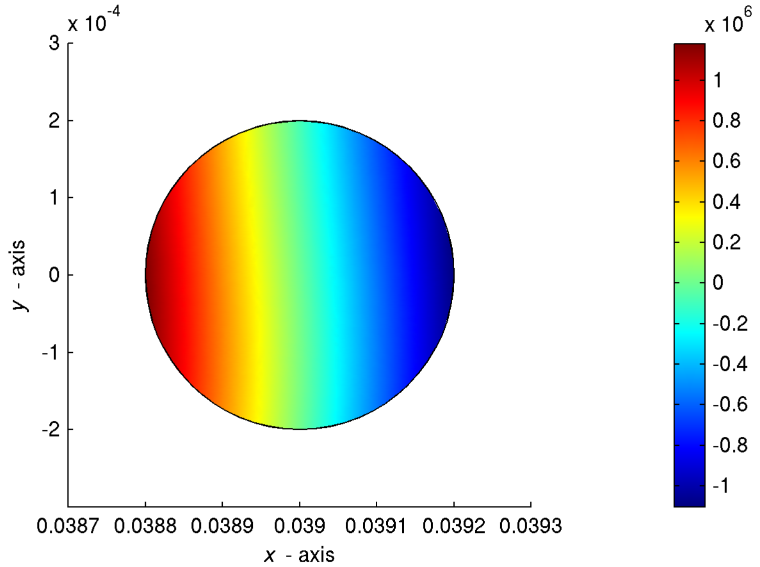

Figure 5.4: Current density in a strand of the stator winding at 30000 r/min.

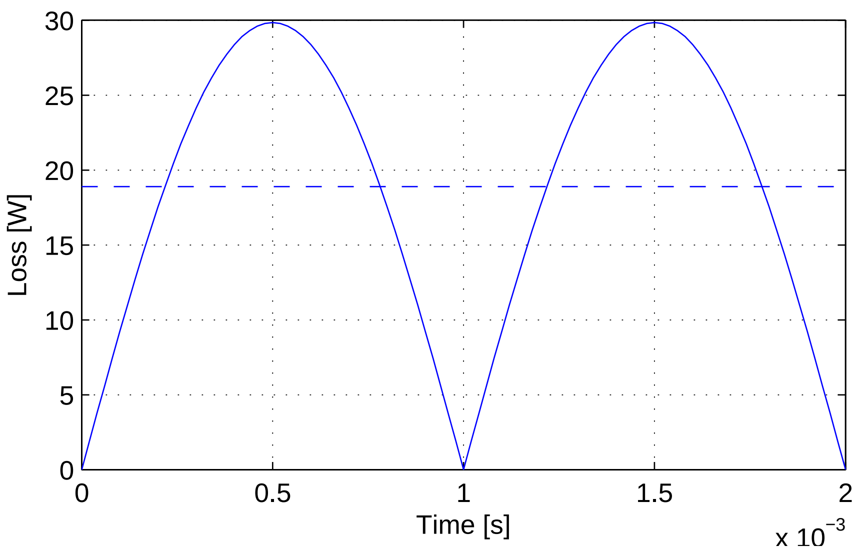

Figure 5.5: Eddy current loss inside the winding

times. More than 4 days [108] and longer than 1000 hours [111] have been reported in literature. Analytical methods have also been used to calculate this loss. Holm used the Poynting vector [13]. Atallah *et al.* used surface integrals in polar coordinates to investigate the effect of circumferential segmenting of the PM and this reduced eddy current loss in the PM significantly [132]. Zhu *et al.* used a DC traction machine to verify the 2-D analytical solution using a current sheet distribution [133].

5.5.2 Resistive model

As discussed in section 2.7.1, eddy currents will be induced in a conductive material whenever a changing magnetic field is established in the material. Eddy currents are induced in the shielding cylinder by all non-fundamental frequency currents flowing in the stator windings. In this section, these eddy currents will be calculated for the worst case senario: when assuming there is perfect coupling between the stator windings and shielding cylinder.

Figure 5.6 shows the direction of current flow in the $r\phi$ - plane (a) and a linear view of the $z\phi$ - plane (b). Assuming a balanced three phase supply and load, if the current in phase a is a maximum positive value ($I_{a,max}$), the current in the b and c phases will be $-0.5I_{a,max}$.

The total eddy current loss can be approximated by conduction loss in the segments shown on the right of Figure 5.6. It is assumed that the current flows in either the axial or tangential direction. The resistance of each reflected phase on the rotor ($R_{r,z}$) in the axial direction can be calculated using

$$R_{r,z} = \frac{L}{\sigma(\delta w_p)} \tag{5.10}$$

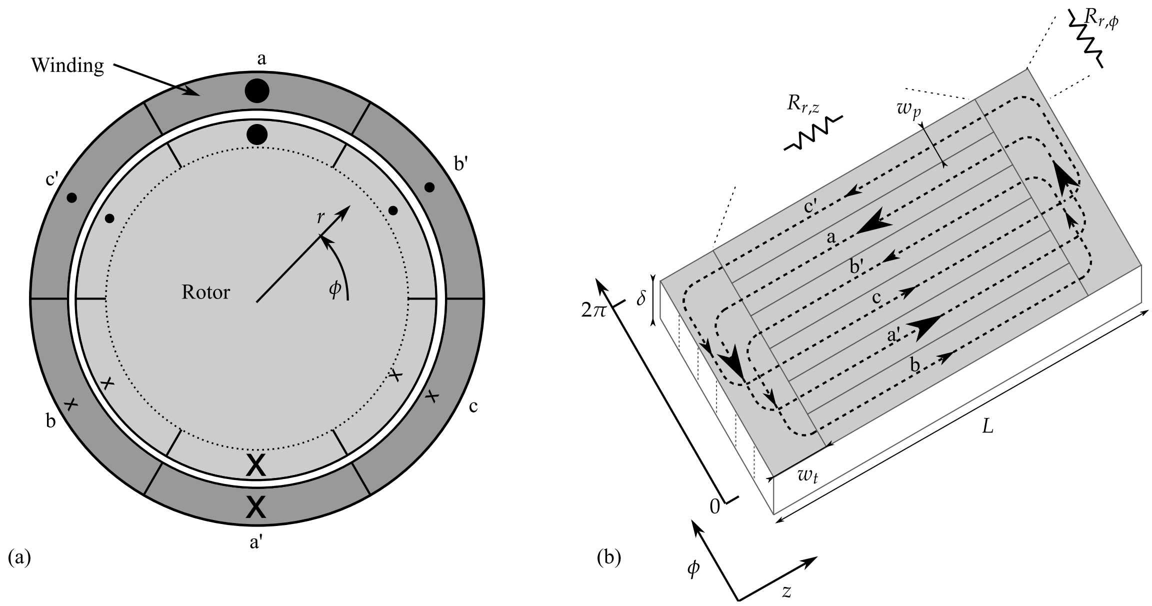

Figure 5.6: Eddy current patterns in rotor of two pole, three phase PMSM: (a) $r\phi$ - plane; and (b) linear $z\phi$ - plane

where L is the axial length of the rotor active region, σ is the electric conductivity, δ is the penetration depth and w_p is the pole width. The current changes direction at the ends of the rotor to flow in the tangential direction and the resistance in this direction ($R_{r,\phi}$) can be calculated using:

$$R_{r,\phi} = \frac{w_p}{\sigma(\delta w_t)} \tag{5.11}$$

were w_t is the width of the part where the current flows in the tangential direction. The frequency of the current will influence the penetration depth in the following way:

$$\delta(f) = \sqrt{\frac{2}{2\pi f \sigma \mu}} = \frac{0.656}{\sqrt{f}} \tag{5.12}$$

since the relative permeability and conductivity of the shielding cylinder and PM material are assumed to be 1 and 588 $\times 10^3$ S/m, respectively. Figure 5.7 shows the penetration depth for frequencies between 400 and 500 000 Hz, which is 30 mm and 0.9 mm, respectively. Both the resistances ($R_{r,z}$ and $R_{r,\phi}$) are inversely proportional to the penetration depth.

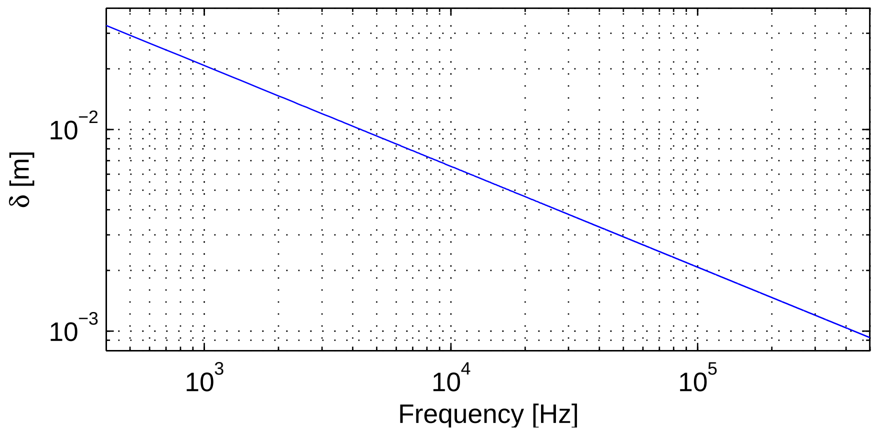

Figure 5.7: Penetration depth of the TWINS' PM and shielding cylinder

The total rotor loss is the sum of the loss due to all the non-fundamental currents, including the harmonics of the rotational frequency as well as the switching frequency and its harmonics. The current at the switching frequency causes significant, high frequency currents when a voltage source inverter (VSI) is used, as is the case with the TWINS. Figure 5.8 shows the equivalent circuit of the rotor eddy currents. Consider an RMS current, $I_{f,rms}$ with frequency f. The eddy current in the z - direction can thus be calculated using

$$I_{f,z} = \sqrt{2 \times \left[I_{f,rms}\right]^2 + 4 \times \left[\frac{1}{2} I_{f,rms}\right]^2} \tag{5.13}$$

since two of the strips (a and a') are conducting the entire current and the rest only half of the current, when balanced three phase is assumed. The current in the ϕ - direction is:

$$I_{f,\phi} = \sqrt{2 \times \left[2 \times \left(\frac{1}{2} I_{f,rms}\right)^2 + 2 \times \left(\frac{3}{2} I_{f,rms}\right)^2 + \left(2 I_{f,rms}\right)^2\right]} \tag{5.14}$$

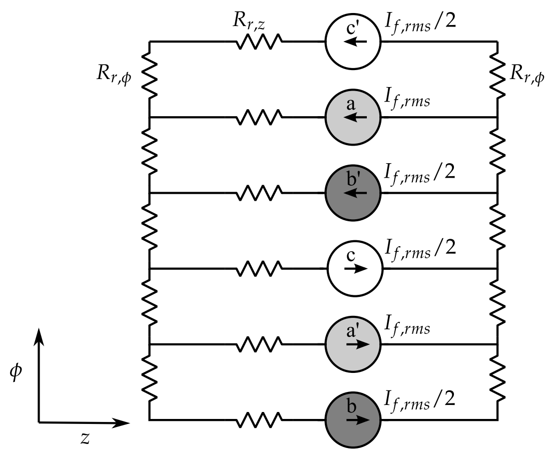

Figure 5.8: Equivalent circuit for rotor eddy currents

This current can be explained using Figure 5.8. Looking at the tangential section of the rotor, only the c′ phase current flows in the upper most tangential resistor, thus only 0.5 $I_{f,rms}$. In the second highest resistor, the currents of phases c′ and a flows, resulting in 1.5 $I_{f,rms}$ there. The same is applied for all the resistors in the tangential section. This is multiplied by two since the current changes direction on both sides of the rotor. The eddy current loss on the rotor due to a current of frequency f can thus be calculated using:

$$P_{f,ec} = I_{f,z}^2 R_{r,z} + I_{f,\phi}^2 R_{r,\phi} \tag{5.15}$$

The total eddy current loss can be calculated by adding the losses due to the different frequencies:

$$P_{tot,ec} = \sum_f P_{f,ec}. \tag{5.16}$$

5.5.3 Rotor eddy current loss in the TWINS

The TWINS will be used as a case study for the proposed eddy current model. Each of the TWINS machines is driven by a VSI with a DC bus voltage of 310 VDC. In this subsection, the expected eddy current loss on the rotor is calculated. It is expected that the eddy current loss at high frequencies will be significant since the penetration depth has a significant effect on the eddy current loss. Only the loss due to the switching frequency are calculated in this section.

Voltage harmonic components

The switching frequency (f_s) of the VSIs used to drive the TWINS is 50 kHz and the fundamental frequency (f_1) is 500 Hz for 30000 r/min. According to Mohan *et al.*, the line to line voltage spectrum is dependent on the frequency modulation ratio (m_f) and amplitude modulation ratio (m_a), which can be calculated using [134]:

$$m_f = \frac{f_s}{f_1} \tag{5.17}$$

and

$$m_a = \frac{\hat{V}_{control}}{\hat{V}_{tri}} \tag{5.18}$$

where $\hat{V}_{control}$ is the maximum value of the control signal and $\hat{V}_{tri}$ is the maximum value of the triangular signal which is compared with the control signal to determine the PWM duty cycle. If $m_a \leq 1$, the VSI operates in the linear region and the TWINS's drives were designed to operate in this region. If $m_a \geq 1$, the VSI operates in a non-linear region which is also referred to as overmodulation. This causes more harmonics in the output voltage which will increase the loss in the machine [134]. Assuming $m_a = 1$, the harmonic components due to the VSI switching in the case of the TWINS are shown in Figure 5.9. The stator winding harmonic currents can be calculated using the stator winding harmonic voltages and stator impedance, which is discussed next.

Stator winding resistance and inductance

The resistance and inductance of the winding are frequency dependent. These parameters can be determined empirically or through electromagnetic models. One example is the analytical model developed by Holm [13]. By applying voltages (or currents) with various fundamental frequencies, and measuring the resulting current and voltage, the frequency dependent resistance and inductance can be determined. A sine, square or triangular voltage (or current) waveform can be used. A square wave contains the fundamental as well as the 3$^{\text{th}}$, 5$^{\text{th}}$, 7$^{\text{th}}$,$\cdots$ harmonics, thus less measurements are required to get a good idea of the stator parameters. A square wave can easily be created with the TWINS' drive and was used to experimentally determine the resistance and inductance of the machine.

The measured current and voltage are transformed to the frequency domain using the fast Fourier transform (FFT) in MATLAB® . Using Ohm's law, the frequency dependent impedance

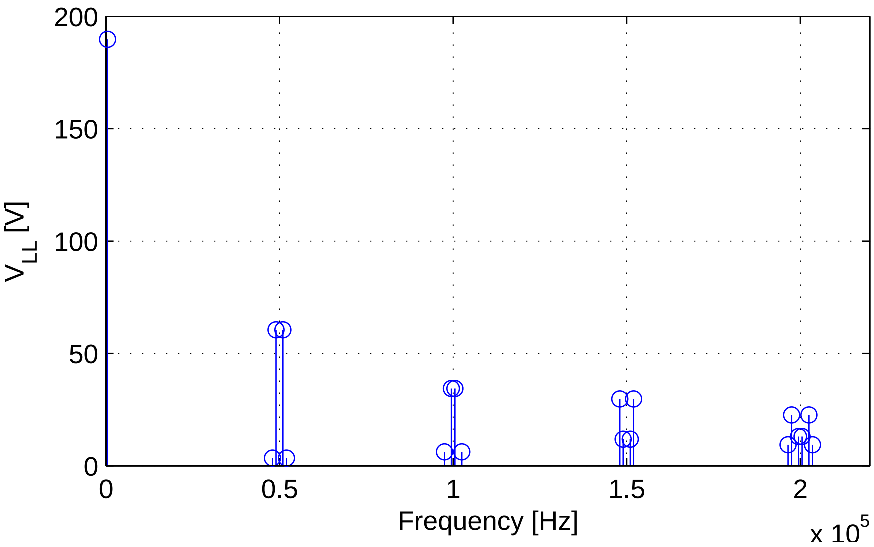

Figure 5.9: VSI harmonic spectrum with $m_a = 1$ [134]

can be calculated. The resistance and inductance are then calculated from the real and imaginary parts of the impedance. Figure 5.10 shows the frequency dependent phase resistance. The resistance can be modelled using two straight lines in the log-log scale:

$$R(f) = \begin{cases} 0.127\ [\Omega] & f \leq 150 \text{ Hz} \\ 10^{-2.21} f^{0.6}\ [\Omega] & f \geq 150 \text{ Hz} \end{cases} \tag{5.19}$$

where f is the frequency. The increase in resistance is a combination of the shielding cylinder loss and the stator iron loss. At the switching frequency and its harmonics, the stator impedance is dominated by the reactance. The mechanisms at work during shielding are discussed in detail by Holm [13] and Polinder [131].

The frequency dependent phase inductance is shown in Figure 5.11. The inductance at low frequencies is 228 μH. Between 100 Hz and 8000 Hz, the inductance decreases by half to 111 μH. It then settles and remains constant as frequency increases. The same behaviour is found in a 300 kW external rotor slotless PMSM [13]. The inductance can be approximated with three straight lines in the log axis:

$$L(f) = \begin{cases} 228\ [\mu\text{H}] & f \leq 250 \text{ Hz} \\ 10^{-3.145} f^{-0.207}\ [\mu\text{H}] & 250 \leq f \leq 8000 \text{ Hz} \\ 111\ [\mu\text{H}] & f \geq 8000 \text{ Hz} \end{cases} \tag{5.20}$$

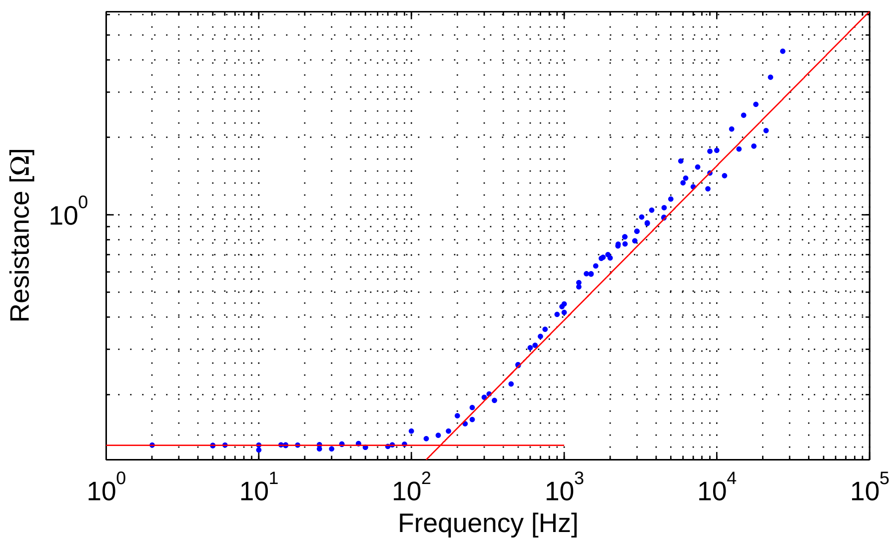

Figure 5.10: Frequency dependent stator resistance (per phase)

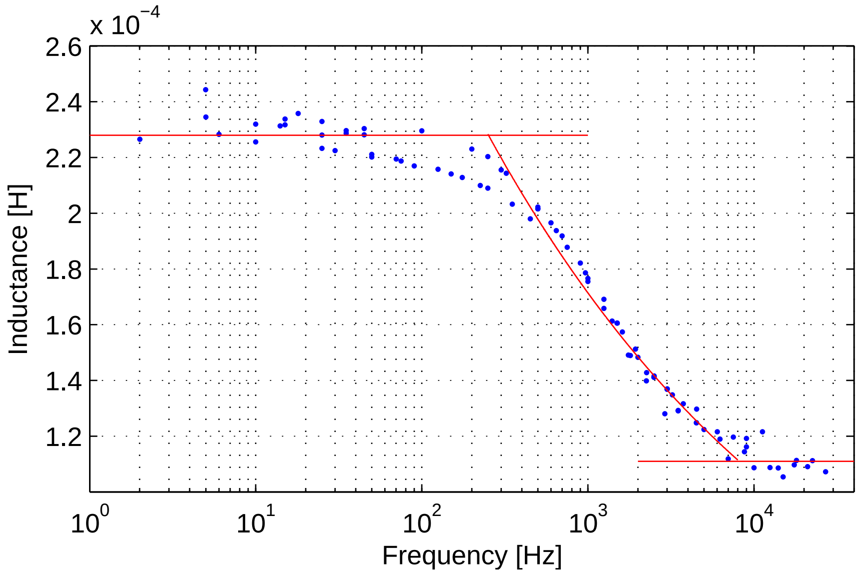

Figure 5.11: Frequency dependent stator inductance(per phase)

Predicted eddy current loss at 30000 r/min

The voltage harmonics and stator winding's impedance can be used to calculate the harmonic currents. At the switching frequency and its harmonics, the stator impedance is dominated by the stator winding's reactance. The frequency dependent impedance must be used at the switching frequency since using the DC impedance would lead to an underestimation of the eddy currents by more than 50 %.

Figure 5.12 shows the influence of the tangential current width (w_t) on the eddy current loss in the rotor due to the VSI switching harmonics. The contribution of the eddy currents flowing in the ϕ and z directions are also shown. The loss due to currents flowing in the z - direction is 4.8 W and those in the ϕ direction decrease when w_t increases. The current flows in the axial and tangential directions on the rotor but the current density also varies in the radial direction. Since all three dimensions are involved, the eddy currents should be modelled in 3-D. In this thesis, w_t is determined using measured rotor temperatures and is discussed in section 6.7.2.

5.6 Mechanical losses

Both types of mechanical losses are a result of friction. In the bearing, there is friction between the moving balls and races. The air inside the air gap resists movement, causing windage loss on the rotor surface.

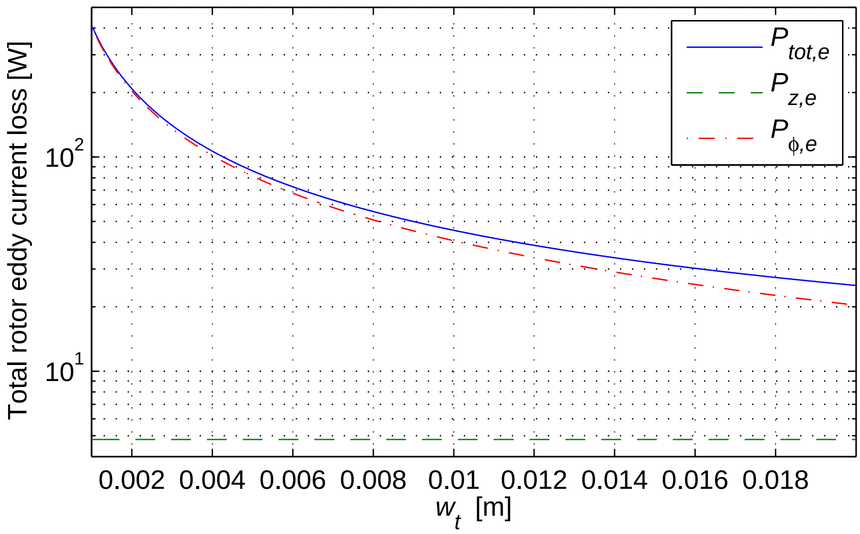

Figure 5.12: Calculated rotor eddy current loss vs. tangential current width (w_t) for f_s=50 kHz VSI harmonics

5.6.1 Bearing loss

The bearing loss is proportional to the rotational speed (ω), friction coefficient of the bearing (k_{fr}), the dynamic load (F) and the bearing ID ($d_{Bearing}$):

$$\begin{aligned} P_{bearing} &= 0.5\omega k_{fr} F d_{Bearing} \\ &= 0.5(2\pi 500)(0.0015)(20)(0.02) \\ &= 0.942 \text{ W} \end{aligned} \tag{5.21}$$

The friction coefficient used is for a bearing with metal balls, instead of the ceramic balls used in the hybrid bearing of the TWINS. This is because k_{fr} is not available for the hybrid bearing used in the TWINS. The bearing loss should be smaller for hybrid bearings, thus this can be seen as a worst case.

5.6.2 Windage loss

The rotor surface friction can be calculated using (2.28). In order to calculate the torque coefficient (C_M), the Reynolds number needs to be determined using (2.16):

$$\begin{aligned}
\mathrm{Re}_D &= \frac{\rho u_m l_A}{\mu} \\
&= \frac{\rho \omega r_{Sc} l_A}{\mu} \\
&= \frac{(1.2)(2\pi 500)(0.0315)(0.5\times 10^{-3})}{18.25\times 10^{-6}} \\
&= 3253.
\end{aligned} \tag{5.22}$$

For this Reynolds number, C_M must be calculated using (2.29c):

$$\begin{aligned}
C_M &= 1.03\frac{(2L_g/d)^{0.3}}{\mathrm{Re}^{0.5}} \\
&= 1.03\frac{\left[(2\times 0.5\times 10^{-3})/0.0315\right]^{0.3}}{3253^{0.5}} \\
&= 6.41\times 10^{-3}.
\end{aligned} \tag{5.23}$$

The surface frictional loss at 30000 r/min in the TWINS is:

$$\begin{aligned}
P_{wind} &= \frac{1}{32}k_s C_M \pi \rho \omega^3 d^4 L \\
&= \frac{1}{32}(1.4)(6.41\times 10^{-3})\pi(1.2)(2\pi 500)^3(0.0315)^4(0.06) \\
&= 1.93\ \mathrm{W}
\end{aligned} \tag{5.24}$$

5.7 Summary of calculated losses

Rotational speed has a significant influence on the losses inside the TWINS, as shown in Figure 5.13. The stator iron and winding eddy current losses are the largest. The advantage of using Litz wire in the stator is thus mainly in reducing eddy current loss in the winding and not necessarily reducing skin effect. There is a quadratic relation of the stator winding eddy current loss and the conductor radius, thus this loss component can be reduced significantly by using thinner wire. Mechanical strength and commonly available wire sizes will limit the reduction possible. The largest loss components shown in Figure 5.13 are located on the stator where it can more easily be removed than on the rotor.

From Figure 5.12 it is clear that the eddy current loss in the rotor will be significant. Even if the tangential current width is a third of the axial length (20 mm), the calculated eddy current loss is still larger than 20 W at 30000 r/min. This will be addressed further in the following two chapters.

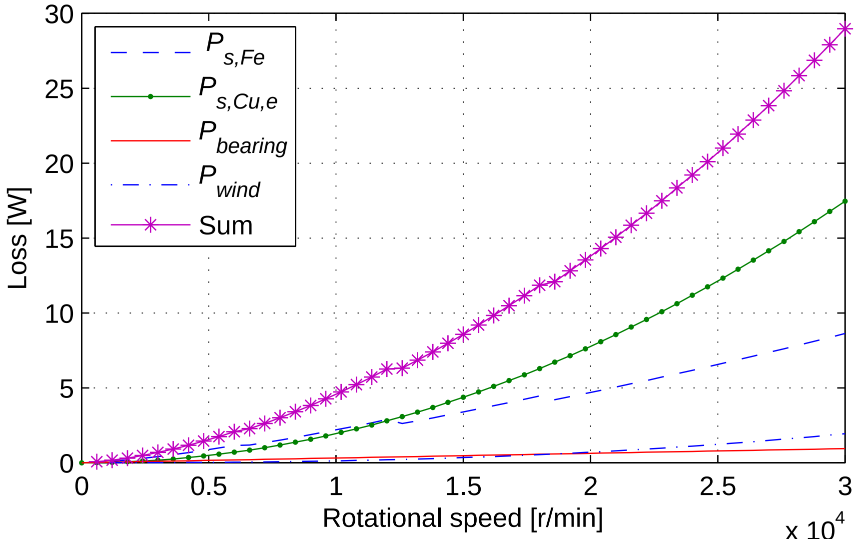

Figure 5.13: Calculated $P_{s,Fe}$, $P_{s,Cu,e}$, $P_{bearing}$, P_{wind} and sum of these losses vs. rotational speed

5.8 Conclusion

Loss modelling is an integral part of thermal modelling, since the heat sources in an electric machine are losses. This chapter discussed the dominant loss mechanisms found in high speed, slotless PMSMs. The stator losses are mainly due to the varying magnetic field caused by the rotor movement. A 2-D analytical model for this field was derived and used to determine the stator iron loss as well as winding eddy current loss. Comparing the winding eddy current loss calculated using the analytical model with FEM predictions showed good correlation.

Eddy current loss on the rotor is caused by non-fundamental currents flowing in the winding. Using a VSI as drive for a PMSM results in large rotor eddy current loss due to high frequency switching. A simple 1-D, resistive model was discussed and it was found that the tangential current width should be investigated.